

Structures of $[(\text{CO}_2)_n(\text{CH}_3\text{OH})_m]^-$ ($n = 1 - 4$, $m = 1, 2$) Cluster Anions

Journal:	<i>The Journal of Physical Chemistry</i>
Manuscript ID:	jp-2008-00289g
Manuscript Type:	Article
Date Submitted by the Author:	12-Jan-2008
Complete List of Authors:	Muraoka, Azusa; The University of Tokyo, Department of Basic Science, Graduate School of Arts & Sciences Inokuchi, Yoshiya; Hiroshima University, Department of Chemistry, Graduate School of Science Nagata, Takashi; The University of Tokyo, Department of Basic Science, Graduate School of Arts & Sciences



Structures of $[(\text{CO}_2)_n(\text{CH}_3\text{OH})_m]^-$ ($n = 1 - 4, m = 1, 2$)

Cluster Anions

*Azusa Muraoka, Yoshiya Inokuchi,[†] and Takashi Nagata**

Department of Basic Science, Graduate School of Arts and Sciences, The University of Tokyo, Komaba,
Meguro-ku, Tokyo 153-8902, Japan

azusa@cluster.c.u-tokyo.ac.jp, y-inokuchi@hiroshima-u.ac.jp, nagata@cluster.c.u-tokyo.ac.jp

RECEIVED DATE (to be automatically inserted after your manuscript is accepted if required according to the journal that you are submitting your paper to)

*Corresponding author. E-mail: nagata@cluster.c.u-tokyo.ac.jp. [†]Present address: Department of Chemistry, Graduate School of Science, Hiroshima University, Kagamiyama, Higashi-Hiroshima, Hiroshima 739-8526, Japan.

1
2
3
4
5 **Abstract.** The infrared photodissociation spectra of $[(\text{CO}_2)_n(\text{CH}_3\text{OH})_m]^-$ ($n = 1 - 4$, $m = 1, 2$) are
6 measured in the $2700 - 3700 \text{ cm}^{-1}$ range. The observed spectra consist of an intense broad band
7 characteristic of hydrogen-bonded OH stretching vibrations at $\approx 3300 \text{ cm}^{-1}$ and congested vibrational
8 bands around 2900 cm^{-1} . No photofragment signal is observed for $[(\text{CO}_2)_{1,2}(\text{CH}_3\text{OH})_1]^-$ in the spectral
9 range studied. *Ab initio* calculations are performed at the MP2/6-311++G** level to obtain structural
10 information such as optimized structures, stabilization energies, and vibrational frequencies of
11 $[(\text{CO}_2)_n(\text{CH}_3\text{OH})_m]^-$. Comparison between the experimental and theoretical results reveals the
12 structural properties of $[(\text{CO}_2)_n(\text{CH}_3\text{OH})_m]^-$: (1) the incorporated CH_3OH interacts directly with either
13 CO_2^- or C_2O_4^- core by forming an $\text{O}-\text{H}\cdots\text{O}$ linkage; (2) the introduction of CH_3OH promotes charge
14 localization in the clusters via the hydrogen-bond formation, resulting in the predominance of
15 $\text{CO}_2^-\cdot(\text{CH}_3\text{OH})_m(\text{CO}_2)_{n-1}$ isomeric forms over $\text{C}_2\text{O}_4^-\cdot(\text{CH}_3\text{OH})_m(\text{CO}_2)_{n-2}$; (iii) the hydroxyl group of
16 CH_3OH provides an additional solvation site for neutral CO_2 molecules.
17
18
19
20
21
22
23
24
25
26
27
28
29
30
31
32

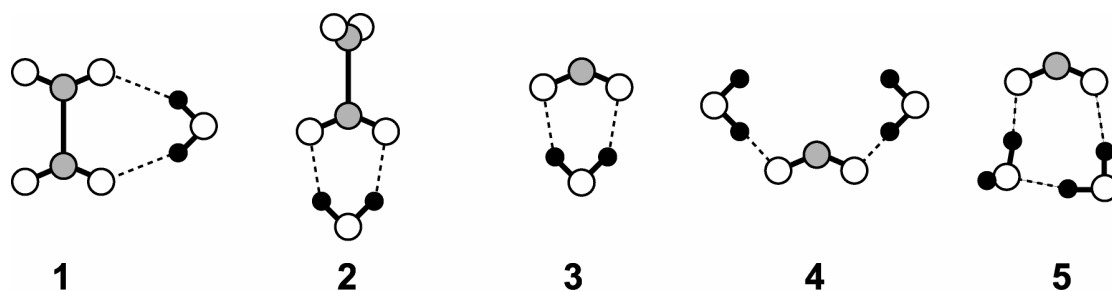
33 **Keywords:** Infrared photodissociation spectroscopy, hydrogen bond, electronic isomer, *ab initio*
34 calculation.
35
36
37
38
39
40
41
42
43
44
45
46
47
48
49
50
51
52
53
54
55
56
57
58
59
60

Introduction

Since the first mass-spectrometric discovery of the hydrated anion of CO₂ by Klots,¹ stabilization of otherwise unstable gas-phase anions by “microhydration” has been a subject of a number of investigations.^{2–9} Unveiling the physics behind the distinct stabilities of those gas-phase hydrated anions eventually leads to the microscopic understandings of various phenomena involving ionic species in solutions. The first step to be taken toward this end is to seek the structural information on the hydrated anions. In our previous study, the structures of [(CO₂)_n(H₂O)_m][–] (*n* = 1 – 4, *m* = 1, 2) were investigated by infrared photodissociation (IPD) spectroscopy combined with *ab initio* calculations.¹⁰ The IPD measurement in the spectral region of hydrogen-bonded OH stretching vibrations (3000 – 3800 cm^{–1}) has revealed rather size- and composition-specific hydration manner in these small [(CO₂)_n(H₂O)_m][–]. The previous findings are summarized as follows: (1) The dominant isomeric forms of [(CO₂)_n(H₂O)₁][–] (*n* = 2 – 4) contain a double ionic hydrogen-bonding (DIHB) configuration composed of C₂O₄[–] and H₂O (configuration 1 or 2 in Scheme 1) as a structural subunit; (2) A DIHB configuration composed of CO₂[–] and H₂O (configuration 3) appears only as a minor subunit in [(CO₂)_n(H₂O)₁][–] (*n* = 2 – 4); (3) Two H₂O molecules make hydrogen bonds independently with the O atoms of CO₂[–] (configuration 4) in [(CO₂)_n(H₂O)₂][–] (*n* = 1, 2); (4) In the series of [(CO₂)_n(H₂O)₂][–], configurations 1 and 2 appear only at *n* = 2; (5) A cyclic structure including CO₂[–] and two H₂O molecules (configuration 5) is formed in [(CO₂)₃(H₂O)₂][–]. For the descriptive convenience, hereafter, the isomeric forms represented as CO₂[–]·(H₂O)_m(CO₂)_{*n*–1} and C₂O₄[–]·(H₂O)_m(CO₂)_{*n*–2} are referred to as “type I” and “type II”, respectively, after Ref. 11. In type I structure, the excess electron is localized on a CO₂ monomer, whereas the electron is delocalized over two CO₂ constituents to form C₂O₄[–] as the anionic core in type II structure. These two forms of [(CO₂)_n(H₂O)_m][–] are designated as “electronic isomers” because they are constitutional isomers having different electronic structures. Although there seems to be no common thread which runs through the hydration manner observed in [(CO₂)_n(H₂O)_m][–], it can be inferred from the above findings that (i) C₂O₄[–] is stabilized always through the formation of a DIHB configuration in [(CO₂)_n(H₂O)_m][–], and that (ii) hydration plays a crucial role to localize the

charge distribution in $[(\text{CO}_2)_n(\text{H}_2\text{O})_m]^-$. The validity of the latter inference is obvious for $m = 2$, while ensured also for $m = 1$ by considering the fact that $(\text{CO}_2)_n^-$ almost exclusively take on type II structure, $\text{C}_2\text{O}_4^- \cdot (\text{CO}_2)_{n-2}$, in the size range $n = 2 - 4$;¹²⁻¹⁴ the incorporation of one H_2O into $(\text{CO}_2)_n^-$ tends to increase the relative abundance of type I structure.^{10, 11}

SCHEME 1



Focusing on the physics behind the stabilization of anions by hydration, one might intuitively infer that the extent of charge delocalization within the cluster is primarily governed by the competition between stabilization attained by solvent-induced charge localization and the intrinsic tendency toward charge delocalization through resonance interactions. As H_2O can interact strongly with charge-concentrated moieties through hydrogen-bond formation, the introduction of H_2O into $(\text{CO}_2)_n^-$ would promote charge localization in the cluster to a considerable extent. Contrary to this expectation, the previous photoelectron spectroscopic study showed that type II structures still dominated in $[(\text{CO}_2)_n(\text{H}_2\text{O})_1]^-$ ($n = 2 - 4$) while type I isomers appeared only as minor species.¹¹ The dominance of type II isomers is also confirmed by the IPD experiment as mentioned above (finding (1)). As readily seen from the structural “motifs” displayed in Scheme 1, the exceptional stability of type II isomers (C_2O_4^- core) is ascribable to the occurrence of configuration 1; this originates from the unique ability of H_2O to form DIHB configurations. Thus, the intrinsic propensity for charge localization by hydrogen-bond formation is somewhat blurred in $[(\text{CO}_2)_n(\text{H}_2\text{O})_m]^-$.

In the present study, we apply IPD spectroscopy to $[(\text{CO}_2)_n(\text{CH}_3\text{OH})_m]^-$ ($n = 1 - 4$, $m = 1, 2$). The IPD spectra are measured in the $2700 - 3700 \text{ cm}^{-1}$ range, providing information on the hydrogen-bonds formed in $[(\text{CO}_2)_n(\text{CH}_3\text{OH})_m]^-$. As CH_3OH can be thought as being the simplest protic molecule with

one hydroxyl group, it is expected that the hydrogen-bonded structures of $[(\text{CO}_2)_n(\text{CH}_3\text{OH})_m]^-$ simply reflect the role of the protic solvent as a charge-localization promoter as well as an anion stabilizer. *Ab initio* calculations for $[(\text{CO}_2)_n(\text{CH}_3\text{OH})_m]^-$ are also performed at the MP2/6-311++G** level. The calculations provide optimized geometries for $[(\text{CO}_2)_n(\text{CH}_3\text{OH})_m]^-$ along with their vibrational frequencies, which can be compared directly with the experimental IPD spectra. Based on the IPD spectral features in conjunction with the *ab initio* results, the structural properties of $[(\text{CO}_2)_n(\text{CH}_3\text{OH})_m]^-$ are discussed in terms of the solvent-induced charge localization and stabilization.

Experimental Section

The IPD spectra of $[(\text{CO}_2)_n(\text{CH}_3\text{OH})_m]^-$ are measured by an ion-guide spectrometer equipped with a tandem quadrupole mass filter.¹⁵ The target $[(\text{CO}_2)_n(\text{CH}_3\text{OH})_m]^-$ is prepared as follows. A gas mixture of carbon dioxide and methanol (a total stagnation pressure of $1 - 2 \times 10^5$ Pa) is introduced into the vacuum chamber through a pulsed nozzle (General Valve Series 9) with a repetition rate of 10 Hz. The pulsed free jet is crossed with a continuous electron beam at the exit of the nozzle, resulting in the production of secondary slow electrons. These electrons are attached to neutral $[(\text{CO}_2)_M(\text{CH}_3\text{OH})_M]$ clusters in the beam to form the $[(\text{CO}_2)_n(\text{CH}_3\text{OH})_m]^-$ cluster anions. After passing through a skimmer, the cluster ions are accelerated into the first quadrupole mass filter by a 50-eV pulsed voltage. Mass-selected ions of interest are then introduced into a quadrupole ion guide through a 90° ion bender. The ion beam is merged with an output of a pulsed infrared photodissociation laser in the ion guide. Resultant fragment ions are mass-analyzed by the second quadrupole mass filter and detected by a secondary electron multiplier tube. The IPD spectra of the parent ions are obtained by plotting the yields of fragment ions against wavenumber of the dissociation laser. The dissociation channel monitored for obtaining the IPD spectra of $[(\text{CO}_2)_n(\text{CH}_3\text{OH})_m]^-$ is the loss of one CO_2 molecule except for $[(\text{CO}_2)_1(\text{CH}_3\text{OH})_2]^-$; one CH_3OH is ejected upon the infrared irradiation on $[(\text{CO}_2)_1(\text{CH}_3\text{OH})_2]^-$.

The tunable infrared source used in this study is an optical parametric oscillator system (Continuum Mirage 3000) pumped with an injection-seeded Nd:YAG laser (Continuum Powerlite 9010). The

1
2
3 output energy is about 1 – 2 mJ pulse⁻¹ with a linewidth of ≈ 1 cm⁻¹. The infrared laser is loosely
4
5 focused into the ion guide by using a CaF₂ lens ($f = 1000$ mm) .
6

7
8 *Ab initio* MO calculations are carried out with the GAUSSIAN 98 program package¹⁶ in order to
9
10 estimate the structural and spectroscopic properties of $[(\text{CO}_2)_n(\text{CH}_3\text{OH})_m]^-$, such as optimized
11
12 geometries, vibrational frequencies and total energies. Geometry optimization and vibrational
13
14 frequency analysis are performed at the MP2/6-31+G* and MP2/6-311++G** levels of theory. Both
15
16 levels of theory have provided primarily identical and consistent results for optimized geometries and
17
18 vibrational frequencies. In this article, we employ the optimized structures and vibrational frequencies
19
20 obtained by the MP2/6-311++G** calculations for spectral assignments. To compare the calculated
21
22 vibrational frequencies with observed ones, a scaling factor of 0.9404 is employed for all the
23
24 vibrational frequencies with observed ones, a scaling factor of 0.9404 is employed for all the
25
26 frequencies calculated. This factor is determined so as to reproduce the OH stretching vibrational
27
28 frequencies of a free CH₃OH molecule. For saving CPU time without sacrificing seriously our pursuit
29
30 of accuracy, the total energies of $[(\text{CO}_2)_n(\text{CH}_3\text{OH})_m]^-$ are evaluated by the single-point energy
31
32 calculations at the CCSD(T)/6-31+G* level with the optimized structures given by the MP2/6-31+G*
33
34 calculations (CCSD(T)/6-31+G*/MP2/6-31+G*).
35
36
37
38

39 **Results and Discussion**

40
41 A. Infrared photodissociation spectra of $[(\text{CO}_2)_n(\text{CH}_3\text{OH})_m]^-$. Figure 1 presents an overview of the
42
43 IPD spectra of $[(\text{CO}_2)_n(\text{CH}_3\text{OH})_m]^-$ with $n = 1 - 4$, and $m = 1, 2$ measured in the 2700 – 3700 cm⁻¹
44
45 range. Except for the $(n, m) = (1, 1)$ and $(2, 1)$ spectra, where the fragment signals were indiscernible,
46
47 the IPD spectra possess similar features in the observed spectral range; i.e., a sharp band at 2800 cm⁻¹, a
48
49 somewhat broad band around 2900 cm⁻¹, and an intense broad band spreading over the range of 3100 –
50
51 3400 cm⁻¹. The similarity in these spectral features, especially in the spectral region associated with the
52
53 OH-stretching vibration (3000 – 3700 cm⁻¹), indicates that the $[(\text{CO}_2)_n(\text{CH}_3\text{OH})_m]^-$ species investigated
54
55 here contain a similar type of hydrogen-bonded structure.
56
57
58
59
60

From the overview displayed in Fig. 1, we infer that the intense broad band at $\approx 3300\text{ cm}^{-1}$ in each spectrum is assignable to the hydrogen-bonded OH stretching vibration of CH_3OH ; the spectral position is shifted significantly toward lower frequencies from that of the OH stretching vibration of gas-phase CH_3OH (3681 cm^{-1})¹⁷. This assignment is further confirmed by checking the absence of the $\approx 3300\text{-cm}^{-1}$ band in the IPD spectra of $[(\text{CO}_2)_n(\text{CH}_3\text{OD})_m]^-$ measured under the identical conditions. The spectral features in the $2800 - 3000\text{ cm}^{-1}$ range are found to be rather insensitive to the size and the composition of $[(\text{CO}_2)_n(\text{CH}_3\text{OH})_m]^-$. We are able to assign the 2800- and 2900-cm^{-1} bands to the vibrations of the methyl group of CH_3OH , based on their spectral positions and the assignments reported in literature.¹⁷ As the $2800 - 3000\text{ cm}^{-1}$ spectral features give only little information on the hydrogen-bonded structures of $[(\text{CO}_2)_n(\text{CH}_3\text{OH})_m]^-$, we will focus our interest on the spectral features in the $3000\text{-}3700\text{-cm}^{-1}$ range hereafter.

B. Spectral assignments

1. $[(\text{CO}_2)_n(\text{CH}_3\text{OH})_1]^-$. Although we could not detect any IPD signal for $[(\text{CO}_2)_1(\text{CH}_3\text{OH})_1]^-$, hydrogen-bonded structures for $[(\text{CO}_2)_1(\text{CH}_3\text{OH})_1]^-$ are still deemed worthy considering as the prototypical ones. As shown in Fig. 2, *ab initio* calculations predict the existence of two stable isomeric forms for $[(\text{CO}_2)_1(\text{CH}_3\text{OH})_1]^-$ at the MP2/6-311++G** level. The structures shown in Fig. 2 are essentially identical to those obtained previously by the MP2/6-31+G* calculations.¹⁸ The isomeric form denoted as 1-1A is the most stable one, while 1-1A and 1-1B are almost equal in energy. The total energies of the isomers differ from each other only by 0.002 eV at the CCSD(T)/6-31+G*/MP2/6-31+G* level. Hereafter, we use the notation “*n-mX*” in referring to each isomeric form, where the first digit of “*n-mX*” represents the number *n* of CO_2 molecules involved in the cluster anion, the second digit the number *m* of CH_3OH molecules, and the last character “X” is for identifying the individual structure. The frequencies of the hydrogen-bonded OH stretching vibrations are calculated to be 3272 and 3218 cm^{-1} for 1-1A and 1-1B, respectively, both of which lie in the spectral range investigated. The absence of IPD signals for $[(\text{CO}_2)_1(\text{CH}_3\text{OH})_1]^-$ is ascribable either to the large bond dissociation energy for the $\text{CO}_2^- + \text{CH}_3\text{OH}$ channel, or to the instability of the possible photoproduct CO_2^- . The

1
2
3 amount of energy required for the hydrogen-bond dissociation is estimated to be 0.67 eV for 1-1A,
4 which is well above the infrared-photon energies employed in the present study ($2700 - 3700 \text{ cm}^{-1}$, 0.33
5 – 0.46 eV). As will be discussed later, however, the $[(\text{CO}_2)_n(\text{CH}_3\text{OH})_m]^-$ species are produced
6 internally “hot” under the present beam conditions. We cannot rule out the possibility that the internally
7 hot species dissociate upon the infrared-photon absorption. If this is the case, the product CO_2^- might
8 elude the detection due possibly to its short lifetime ($<100 \mu\text{s}^{19}$).
9

10
11 As already seen in Fig. 1, also $[(\text{CO}_2)_2(\text{CH}_3\text{OH})_1]^-$ does not provide IPD signals. The present *ab*
12 *initio* calculations predict the existence of eight stable isomeric forms for $[(\text{CO}_2)_2(\text{CH}_3\text{OH})_1]^-$ at the
13 MP2/6-311++G** level. In Fig. 3 shown are three of them as the lowest-energy representatives of the
14 isomeric forms having different hydrogen-bonded structures. Forms 2-1B and 2-1C belongs to type I
15 structure (CO_2^- core), and 2-1A to type II structure (C_2O_4^- core). While 2-1A is the global minimum
16 structure, 2-1A and 2-1B are almost isoenergetic. The energy difference, ΔE , is 0.008 eV at the
17 CCSD(T)/6-31+G**//MP2/6-31+G* level, where ΔE is defined as the amount of total energy with
18 respect to the global minimum structure. For 2-1C, ΔE is calculated to be 0.069 eV. The calculations
19 predict the bond dissociation energy for the least energy-demanding channel, $[(\text{CO}_2)_2(\text{CH}_3\text{OH})_1]^- \rightarrow$
20 $\text{CO}_2^- \cdot \text{CH}_3\text{OH} + \text{CO}_2$, to be 0.40, 0.39 and 0.33 eV for 2-1A, 2-1B and 2-1C, respectively. The
21 calculated frequencies of the hydrogen-bonded OH stretching vibrations are 3512 cm^{-1} for 2-1A, 3209
22 cm^{-1} for 2-1B, and 3182 cm^{-1} for 2-1C. Apparently, the absence of IPD signals cannot be elucidated in
23 terms of the bond dissociation energies and the spectral positions. At the present stage, this issue
24 remains to be explained.
25
26
27
28
29
30
31
32
33
34
35
36
37
38
39
40
41
42
43
44
45
46
47
48

49 The $[(\text{CO}_2)_3(\text{CH}_3\text{OH})_1]^-$ anion is the smallest member of $[(\text{CO}_2)_m(\text{CH}_3\text{OH})_1]^-$ series which undergoes
50 vibrational predissociation into fragment anions via the infrared excitation. The IPD signals were
51 detected as the loss of one CO_2 from $[(\text{CO}_2)_3(\text{CH}_3\text{OH})_1]^-$. In Fig. 4 the IPD spectrum of
52 $[(\text{CO}_2)_3(\text{CH}_3\text{OH})_1]^-$ in the $3000 - 3700 \text{ cm}^{-1}$ range is compared with the vibrational spectra calculated
53 for possible isomeric forms. The main band of the IPD spectrum is composed of at least two
54 components, one of which is located at 3244 cm^{-1} and the other at $\approx 3170 \text{ cm}^{-1}$ as a shoulder. Besides
55
56
57
58
59
60

1
2
3 these bands, tiny peaks appear at 3436 and 3507 cm^{-1} . Considering that each band component
4 corresponds to the specific OH oscillation of a certain isomeric form, we can infer that at least four
5 types of isomeric forms contribute to the observed IPD spectrum. The MP2/6-311++G** calculations
6 provide 23 possible geometries for $[(\text{CO}_2)_3(\text{CH}_3\text{OH})_1]^-$; 18 isomers belong to type I and the remaining
7 five are of type II structure. In all these calculated isomeric forms, a hydrogen bond is formed between
8 CH_3OH and the O atom of either the CO_2^- or the C_2O_4^- core. In Fig. 4 also shown are the five
9 representative isomeric forms taking on different types of solvation structures. Form 3-1A is the global
10 minimum structure, where CH_3OH interacts with the CO_2^- core through an $\text{OH}\cdots\text{O}$ hydrogen bond and
11 two CO_2 act as solvent interacting directly with the ionic core. As is the case with $(\text{CO}_2)_n^-$, the solvent-
12 core interaction arises from an effective overlap between the $2\pi_u$ (LUMO) orbital of CO_2 and either the
13 $4b_2$ (HOMO) or the $6a_1$ (SOMO) orbital of CO_2^- .²⁰ The $4b_2$ orbital is localized on the O atoms of CO_2^- .
14 The $6b_2$ orbital, primarily localized on the C atom of CO_2^- , extends its electron lobe mainly along the
15 bisector of the angle $\angle\text{OCO}$. This solvent-core interaction scheme gives a qualitative understanding of
16 the solvation structures of 3-1A. In 3-1B ($\Delta E = 0.027$ eV) one neutral CO_2 interacts with the O atom of
17 CH_3OH instead of CO_2^- , while in 3-1C ($\Delta E = 0.065$ eV) two CO_2 do. In the type II isomers, 3-1D (ΔE
18 $= 0.058$ eV) and 3-1E ($\Delta E = 0.089$ eV), the CO_2 solvent attaches either to the C_2O_4^- core or to the O site
19 of CH_3OH . As represented by 3-1A – 3-1E, the solvation structures are eventually categorized
20 according to (1) the type of ionic core and (2) the number of CO_2 molecules attached to CH_3OH .
21 Referring to each category of solvation structures, we introduce a new notation, T^i , where T (= I or II)
22 represents the type of ionic core (CO_2^- or C_2O_4^-) and the suffix i is the number of CO_2 interacting with
23 CH_3OH . For example, the structural category of 3-1A is referred to as I^0 , and that of 3-1E as II^1 . The
24 *ab initio* calculations also reveals that frequencies of the OH stretching vibration are almost same for the
25 isomeric forms belonging to the same category of solvation structure.

26
27
28
29
30
31
32
33
34
35
36
37
38
39
40
41
42
43
44
45
46
47
48
49
50
51
52
53
54
55
56
57
58
59
60
Getting back to the comparison between the observed IPD spectrum and the calculated ones in Fig. 4,
the 3244- cm^{-1} band is ascribable to 3-1A, based on its spectral position. The position of the weak
shoulder (3172 cm^{-1}) coincides fairly well with the calculated frequency of the OH vibration of 3-1B

(3182 cm^{-1}). The 3436 and 3507 cm^{-1} bands are ascribable to the type II isomers, 3-1E and 3-1D, of which calculated frequencies are 3463 and 3526 cm^{-1} . As no discernible vibrational band appears around the spectral position expected for 3-1C (3020 cm^{-1}), we infer that 3-1C has negligible population in $[(\text{CO}_2)_3(\text{CH}_3\text{OH})_1]^-$. Note that 3-1A, 3-1B, 3-1D and 3-1E are the minimum energy representatives of the I^0 , I^1 , II^0 and II^1 families of $[(\text{CO}_2)_3(\text{CH}_3\text{OH})_1]^-$, respectively. For example, the *ab initio* calculations provide five isomeric forms ($\Delta E = 0.01 - 0.05$ eV), other than 3-1A, belonging to I^0 ; their calculated OH vibrational frequencies are located in the range 3250 – 3280 cm^{-1} . Hence, we infer that these I^0 family members as well as 3-1A contribute to the observed broad band at 3244 cm^{-1} . The situation should be the same with 3-1B, 3-1D and 3-1E: not only the minimum-energy structure of each family but also the low-lying family members serve as spectral carriers.

From the above spectral assignments for $[(\text{CO}_2)_3(\text{CH}_3\text{OH})_1]^-$, one can derive some sort of propensity rules regarding the spectral positions: (1) OH oscillator interacting with CO_2^- vibrates at a lower frequency than that interacting with C_2O_4^- ; (2) Addition of one CO_2 on the OH oscillator reduces the frequency by 60 – 70 cm^{-1} , irrespective of the type of interacting ionic core. Item (1) is due possibly to the fact that the OH oscillator interacts through an $\text{OH}\cdots\text{O}$ linkage more strongly with the CO_2^- core because the negative charge is concentrated on the O atoms more in CO_2^- (Mulliken charge ≈ -0.6) than in C_2O_4^- (≈ -0.4). There seems to be no straightforward explanation for item (2). These propensity rules are also applicable to other $[(\text{CO}_2)_n(\text{CH}_3\text{OH})_m]^-$ systems, as will be discussed below.

It is also interesting to note that type II isomers, 3-1D and 3-1E, are detected in the present measurement, although the previous photoelectron spectroscopic study gave no evidence for the existence of type II isomers in $[(\text{CO}_2)_3(\text{CH}_3\text{OH})_1]^-$.¹¹ The IRD measurement proves to be more sensitive to the presence of electronic isomers in $[(\text{CO}_2)_n(\text{CH}_3\text{OH})_m]^-$, as has been already demonstrated by Shin *et al.* in the $(\text{CO}_2)_n^-$ study.¹⁴

As for the $[(\text{CO}_2)_4(\text{CH}_3\text{OH})_1]^-$ species, we could not complete *ab initio* calculations due firstly to a formidable computational time at the MP2/6-311++G** level, and secondly to the increasing number of possible isomeric forms for $[(\text{CO}_2)_4(\text{CH}_3\text{OH})_1]^-$. This prevents us from a direct comparison between

1
2
3 observed and calculated spectra in the $n = 4$ case. The observed $[(\text{CO}_2)_4(\text{CH}_3\text{OH})_1]^-$ spectrum consists
4 of two components at 3212 and 3274 cm^{-1} (Fig. 1). By comparing the spectral features between
5 $[(\text{CO}_2)_3(\text{CH}_3\text{OH})_1]^-$ and $[(\text{CO}_2)_4(\text{CH}_3\text{OH})_1]^-$, and considering the above propensity rules, we assign the
6 3212- and 3274- cm^{-1} components respectively to the hydrogen-bonded OH vibrations of the I^1 and I^0
7 family members of $[(\text{CO}_2)_4(\text{CH}_3\text{OH})_1]^-$.
8
9

10
11
12 **2. $[(\text{CO}_2)_n(\text{CH}_3\text{OH})_2]^-$.** The $[(\text{CO}_2)_1(\text{CH}_3\text{OH})_2]^-$ spectrum is characterized by a remarkably
13 broadened band around 3350 cm^{-1} (Fig. 5), which cannot be resolved into components. Among twelve
14 isomeric forms predicted by the MP2/6-311++G** calculations, three forms are selectively quoted in
15 Fig. 5; they are the lowest-energy representatives of the $[(\text{CO}_2)_1(\text{CH}_3\text{OH})_2]^-$ isomers with different
16 solvation structures. All these isomeric forms gain their stabilization energies by forming two hydrogen
17 bonds. In isomer 1-2A one hydrogen bond is formed between the CO_2^- core and CH_3OH , while the
18 other between two CH_3OH molecules. In 1-2B the O atoms on both sides of the CO_2^- core take part in
19 the hydrogen-bond formation with two CH_3OH molecules, while both CH_3OH make O-H...O linkages
20 with the O atom on one side of the ionic core in 1-2C. Although the CCSD(T)/6-31+G* calculations
21 refer to 1-2A as the global minimum structure, isomers 1-2A – 1-2C are almost isoenergetic: ΔE is
22 calculated to be 0.008 eV for 1-2B, and 0.009 eV for 1-2C.
23
24
25
26
27
28
29
30
31
32
33
34
35
36
37
38

39 As readily seen in Fig. 5, the calculated spectral patterns for 1-2B (3336, 3361 cm^{-1}) and 1-2C (3304,
40 3345 cm^{-1}) reasonably match the IPD spectral features. The position of the higher-frequency band of 1-
41 2A (3375 cm^{-1}) almost coincides with the observed value of $\approx 3350 \text{ cm}^{-1}$, whereas the other vibrational
42 transition expected to occur at 3075 cm^{-1} is not observed in the present measurement. Hence, the
43 observed IPD band is assigned eventually to the hydrogen-bonded OH oscillations of 1-2B, 1-2C and
44 their isomer families. A noteworthy feature of the vibration motions in 1-2B and 1-2C is that two OH
45 oscillators are coupled together forming either an in-phase or an out-of-phase hydrogen-bonded OH
46 stretching vibrational mode. In the in-phase mode two H atoms move back and forth along their O-
47 H...O linkages in a coherent manner, which gives rise to the 3361- cm^{-1} transition for 1-2B, and 3344-
48 cm^{-1} for 1-2C. In the out-of-phase mode one O-H bond stretches during the other compresses; this
49
50
51
52
53
54
55
56
57
58
59
60

mode corresponds to the 3335-cm⁻¹ band of 1-2B, and the 3304-cm⁻¹ band of 1-2C. The large oscillator strength for the 3361-cm⁻¹ transition arises possibly from a large magnitude of ($\partial\mu/\partial Q_i$) for the in-phase O–H stretching motions in 1-2B.

The infrared-photodissociation of $[(\text{CO}_2)_1(\text{CH}_3\text{OH})_2]^-$ occurs with a loss of one CH₃OH in the present study. The threshold energy for $[(\text{CO}_2)_1(\text{CH}_3\text{OH})_2]^- \rightarrow [(\text{CO}_2)_1(\text{CH}_3\text{OH})_1]^- + \text{CH}_3\text{OH}$ is calculated to be 0.67 eV for 1-2B, and 0.64 eV for 1-2C; these values substantially exceed the energy delivered by the 2700 – 3700 cm⁻¹ infrared photons. As multiphoton processes scarcely occur under the present experimental conditions, where the photon density is kept below $\approx 10 \text{ mJ}\cdot\text{cm}^{-2}$, the observation of the IPD spectrum suggests that $[(\text{CO}_2)_1(\text{CH}_3\text{OH})_2]^-$ species prepared in the electron-impact ionized jet carry internal energy enough to dissociate upon the absorption of 2700 – 3700-cm⁻¹ single photon. This might also cause the broadness of the IPD band in the $[(\text{CO}_2)_1(\text{CH}_3\text{OH})_2]^-$ spectrum. Not only the hot bands of specific isomers such as 1-2B and 1-2C but also the vibrational bands of all the isomeric forms with small ΔE can contribute to the IPD spectral features.

The $[(\text{CO}_2)_2(\text{CH}_3\text{OH})_2]^-$ spectrum exhibits an IPD band at 3288 cm⁻¹, which is accompanied by a shoulder at $\approx 3200 \text{ cm}^{-1}$ (Fig. 6). The spectral shape of the 3288-cm⁻¹ band is much sharper than that of $[(\text{CO}_2)_1(\text{CH}_3\text{OH})_2]^-$ and rather resembles the 3244-cm⁻¹ band shape of $[(\text{CO}_2)_3(\text{CH}_3\text{OH})_1]^-$ (see Fig. 4). From this observation we infer that each CH₃OH molecule interacts directly with the CO₂⁻ core via a hydrogen bond, and consequently that the propensity rules proposed in the previous section is applicable to the $[(\text{CO}_2)_2(\text{CH}_3\text{OH})_2]^-$ case. According to the propensity rules, it can be inferred that type II isomers, whose vibrational bands would otherwise appear around 3500 cm⁻¹, make a negligible contribution to the $[(\text{CO}_2)_2(\text{CH}_3\text{OH})_2]^-$ spectrum. In the geometry optimization at the MP2/6-311++G** level, 34 possible isomeric forms are obtained for $[(\text{CO}_2)_2(\text{CH}_3\text{OH})_2]^-$; 27 isomers out of them have type I structure and the remaining seven have type II structure. Among these type I isomers, 17 forms meet the above condition that both CH₃OH are hydrogen-bonded directly to CO₂⁻. In Fig. 6 shown are the representatives for the 17 isomeric forms. As is the case with $[(\text{CO}_2)_1(\text{CH}_3\text{OH})_2]^-$, two CH₃OH molecules are separately hydrogen-bonded to the O atoms on each side of CO₂⁻ (isomer 2-2A,

1
2
3 2-2C), or together to the O atom on one side of CO_2^- (isomer 2-2B, 2-2D). Isomer 2-2A and 2-2C differ
4
5 in the position of CO_2 solvation: neutral CO_2 interacts with the CO_2^- core in 2-2A (category I⁰), while
6
7 with the hydroxyl group of CH_3OH in 2-2C (category I¹). The situation is the same with 2-2B and 2-2D.
8
9 The global minimum structure is 2-2A; the energy ordering is 2-2A < 2-2B ($\Delta E = 0.028$ eV) < 2-2D
10
11 (0.066 eV) < 2-2C (0.070 eV). From the comparison between observed and calculated spectra in Fig. 6,
12
13 we conclude that the IPD bands are ascribable to the $[(\text{CO}_2)_2(\text{CH}_3\text{OH})_2]^-$ isomeric forms as typified by
14
15 2-2A – 2-2D. The infrared-photodissociation of $[(\text{CO}_2)_2(\text{CH}_3\text{OH})_2]^-$ leads to the production of
16
17 $[(\text{CO}_2)_1(\text{CH}_3\text{OH})_2]^-$ fragments, which is consistent with the *ab initio* results: the threshold energy for
18
19 $[(\text{CO}_2)_2(\text{CH}_3\text{OH})_2]^- \rightarrow [(\text{CO}_2)_1(\text{CH}_3\text{OH})_2]^- + \text{CO}_2$ is calculated to be in the range of 0.33 – 0.40 eV for
20
21 2-2A – 2-2D.
22
23
24
25

26 Moving on to $[(\text{CO}_2)_n(\text{CH}_3\text{OH})_2]^-$ with $n = 3$ and 4, we see from Fig. 1 that the main features of the
27
28 IPD spectra displayed in $n = 1$ and 2 still remain in the large- n species although the band profiles are
29
30 somewhat broadened. This implies that the hydrogen-bonded structures emerging in the $n = 1$ and 2
31
32 species retain their motifs in the larger $[(\text{CO}_2)_n(\text{CH}_3\text{OH})_2]^-$ with $n = 3$ and 4. The broadness of the IPD
33
34 bands in the $[(\text{CO}_2)_{3,4}(\text{CH}_3\text{OH})_2]^-$ spectra arises possibly from the increasing number of coexisting
35
36 isomers which undergo vibrational transitions around 3300 cm^{-1} . We have not performed *ab initio*
37
38 calculations for these larger cluster anions; their geometry optimization and frequency analysis are
39
40 definitely beyond our computational ability.
41
42
43

44 **C. Structural evolution in $[(\text{CO}_2)_n(\text{CH}_3\text{OH})_m]^-$.** Summarizing the spectral assignments discussed
45
46 above, solvation structures formed in $[(\text{CO}_2)_n(\text{CH}_3\text{OH})_m]^-$ ($n = 1 - 4$, $m = 1, 2$) are characterized as
47
48 follows: (i) each CH_3OH is hydrogen-bonded directly to the O atom of either CO_2^- or C_2O_4^- core; (ii)
49
50 the CH_3OH solvation tends to stabilize CO_2^- more efficiently than C_2O_4^- , leading to the predominance
51
52 of type I isomers over type II at $(n, m) = (3, 1), (4, 1), (2, 2), (3, 2)$ and $(4, 2)$; (iii) the hydroxyl group of
53
54 CH_3OH provides an additional solvation site for CO_2 attachment. These characteristics mark a sharp
55
56 contrast with those of $[(\text{CO}_2)_n(\text{H}_2\text{O})_m]^-$, especially in terms of core stabilization. In $[(\text{CO}_2)_n(\text{H}_2\text{O})_m]^-$
57
58 with $(n, m) = (2, 1), (3, 1)$ and $(2, 2)$, C_2O_4^- is preferentially stabilized by forming a double ionic
59
60

1
2
3 hydrogen-bonding (DIHB) configuration, where H₂O bridges two CO₂ moieties of the C₂O₄⁻ core so as
4
5 to reinforce the C–C bond formation (configuration 1).¹⁰ Thus, decreasing populations of type II
6
7 isomers in [(CO₂)_n(CH₃OH)_m]⁻ can be attributed to the intrinsic inability of CH₃OH to form a DIHB
8
9 configuration.

10
11 Another aspect of the solvation structures that should be dealt with here is the structural evolution in
12
13 [(CO₂)_n(CH₃OH)_m]⁻ with increase of the number of neutral CO₂. Figure 7 shows the IPD spectra for
14
15 [(CO₂)_n(CH₃OH)₁]⁻ with $n = 4 - 7$ in the 3000 – 3700 cm⁻¹ range. As an aid for further discussion,
16
17 spectral deconvolution processing has been performed and the results are displayed in Fig. 7: the profile
18
19 of each IPD band is approximately reproduced by a superposition of two or three Lorentzian functions,
20
21 each of which corresponds to the OH vibration inherent to a specific hydrogen-bonded structure. As
22
23 has been discussed in section B.2, the components labeled with “0” and “1” in the top panel of Fig. 7
24
25 are assignable to the hydrogen-bonded OH vibrations in [(CO₂)₄(CH₃OH)₁]⁻ isomers having I⁰ and I¹
26
27 structures, respectively. The deconvolution processing has also revealed the existence of a tiny but
28
29 significant component at ≈3100 cm⁻¹ in the $n = 4$ spectrum. This component can be assigned to a
30
31 hydrogen-bonded OH vibration of CH₃OH with two CO₂ interacting with the O atom of the hydroxyl
32
33 group, based on the propensity rules for spectral shifts by CO₂ solvation. Hence, we infer that there
34
35 exist $n = 4$ isomeric forms which belong to a structural category labeled as I² according to the Tⁱ
36
37 nomenclature. As for $n = 5$ and 6, the IPD bands consist of three Lorentzian components ascribable to
38
39 the solvation structures of categories I⁰, I¹ and I², respectively, as is the case with $n = 4$. The spectral
40
41 position of each component sifts toward higher frequencies with increasing the number n : for example,
42
43 the band center of I⁰ component is located at 3274 cm⁻¹ for $n = 4$, 3302 cm⁻¹ for $n = 5$ and 3326 cm⁻¹
44
45 for $n = 6$. This spectral shift arises possibly from the decreasing charge concentration on the CO₂⁻ core
46
47 with increasing the number of solvating molecules; the more the charge is delocalized by solvation, the
48
49 more the hydrogen bond weakens and, as a result, the OH stretching frequency is increased.

50
51 It is interesting to note that the relative intensities of three Lorentzian components at each cluster size
52
53 also change with n , indicating that the relative abundance of I⁰, I¹ and I² structures depend on the cluster
54
55
56
57
58
59
60

1
2
3 size. The isomers in category I^0 has a largest population at $n = 4$, while the population is significantly
4 reduced at $n = 6$. The isomers in category I^2 show an opposite behavior, as clearly seen in Fig. 7. From
5 these observations, it can be inferred that the solvation structures of $[(CO_2)_n(CH_3OH)_1]^-$ evolve with n
6 in such a way that I^0 structures are preferred more in smaller sizes with $n \leq 5$ whereas I^2 structures
7 become dominant in the size range $n \geq 6$. In the $n = 7$ spectrum the intensity of I^0 component becomes
8 negligible. The negligible population – or rather the absence – of I^0 structures suggests that the first
9 solvation shell around the $OCO^- \cdots HOCH_3$ unit is closed at $n = 7$. In the shell-closed structure of
10 $[(CO_2)_7(CH_3OH)_1]^-$, one CO_2 plays a role of the ionic core making an $O \cdots HO$ hydrogen bond with
11 CH_3OH , another CO_2 interacts with the O atom of the OH group, and the remaining five CO_2 neutrals
12 occupy the solvation sites around the CO_2^- core.
13
14
15
16
17
18
19
20
21
22
23
24
25
26
27

28 Conclusion

29
30 In summary, we report on the infrared photodissociation (IPD) spectra of binary cluster anions
31 composed of carbon dioxide and methanol, $[(CO_2)_n(CH_3OH)_m]^-$ ($n = 1 - 4$, $m = 1, 2$). All the observed
32 IPD spectra, except for $(n, m) = (1, 1)$ and $(1, 2)$, are characterized by intense broad bands around 3300
33 cm^{-1} , which are assigned to the hydrogen-bonded OH stretching vibrations of CH_3OH . The $(1, 1)$ and
34 $(1, 2)$ species provide no photofragment signal in the spectral range investigated. *Ab initio* MO
35 calculations have been carried out in order to obtain the optimized structures, vibrational frequencies,
36 and total energies of $[(CO_2)_n(CH_3OH)_m]^-$. The spectral analyses with the aid of the *ab initio* results
37 reveal that $[(CO_2)_n(CH_3OH)_m]^-$ isomeric forms responsible for the observed IPD spectra take on distinct
38 structural motifs, where all the CH_3OH molecules are directly bonded to either CO_2^- or $C_2O_4^-$ core via
39 $O-H \cdots O$ hydrogen linkage(s). It is also revealed that type I structures (CO_2^- core) are preferentially
40 stabilized by CH_3OH solvation in all the $[(CO_2)_n(CH_3OH)_m]^-$ species which undergo infrared-
41 photodissociation in the present study. The IPD bands ascribable to type II isomers ($C_2O_4^-$ core) are
42 observed only at $(n, m) = (3, 1)$. This shows a striking contrast with the $[(CO_2)_n(H_2O)_m]^-$ case, where
43 type II isomers appear as dominant species at $(n, m) = (2, 1)$, $(3, 1)$ and $(4, 1)$. The abundance of type I
44
45
46
47
48
49
50
51
52
53
54
55
56
57
58
59
60

1
2
3 isomers in $[(\text{CO}_2)_n(\text{CH}_3\text{OH})_m]^-$ arises mainly from the fact that localization of the excess charge in the
4
5 CO_2^- moiety, rather than delocalization over C_2O_4^- , is favorable for strong hydrogen-bond formation.
6
7 The findings in the present study exhibit firstly the intrinsic ability of a hydrogen bond to influence the
8
9 charge localization/delocalization in molecular aggregates, and secondly demonstrate afresh the unique
10
11 ability of water as a solvent to form DIHB configurations.
12
13

14
15 **Acknowledgement.** The authors are grateful to Professor K. Takatsuka for the loan of high-
16
17 performance computers, which enabled us to carry out a large amount of calculations. Professor H.
18
19 Ushiyama and Dr. Y. Arasaki are also acknowledged for their technical help in the computation. Part of
20
21 the *ab initio* calculations were performed by using the computer systems (NEC SX-7) at Research
22
23 Center for Computational Science, Okazaki Research Facilities, National Institutes of Natural Sciences
24
25 (NINS). This work was supported by Grants-in-Aid for Scientific Research (Grant Nos. 18550007 and
26
27 19029011) from Japan Society for the Promotion of Science (JSPS), and from the Ministry of Education,
28
29 Culture, Sports, Science and Technology (MEXT).
30
31
32

33
34 **Supporting Information Available:** Structure parameters for the $[(\text{CO}_2)_n(\text{CH}_3\text{OH})_m]^-$ isomeric forms
35
36 shown in Figs. 2 – 6 (MP2/6-311++G**). This material is available free of charge via the Internet at
37
38 <http://pubs.acs.org>. The structure parameters for all the isomeric forms obtained in the present study are
39
40 also available on request; the total numbers of optimized structures are 2, 10, 23, 12 and 34 for $(n, m) =$
41
42 $(1, 1), (2, 1), (3, 1), (1, 2)$ and $(2, 2)$, respectively.
43
44
45
46
47
48

49 50 51 52 53 54 55 56 57 58 59 60 References

- (1) Klots, C. E.; *J. Chem. Phys.* **1979**, 71, 4172.
- (2) Desfrancois, C.; Abdoul-Carime, H.; Schermann, J. P. *J. Chem. Phys.* **1996**, 104, 7792.
- (3) Hendricks, J. H.; Lyapustina, S. A.; de Clercq, H. L.; Bowen, K. H. *J. Chem. Phys.* **1998**, 108, 8.

- 1
2
3 (4) Schiedt, J.; Weinkauf, R.; Neumark, D. M.; Schlag, E. W. *Chem. Phys.* **1998**, 239, 511.
4
5
6 (5) Han, S. Y.; Song, J. K.; Kim, J. H.; Oh, H. B.; Kim, S. K. *J. Chem. Phys.* **1999**, 111, 4041.
7
8
9 (6) Periquet, V.; Moreau, A.; Carles, S.; Schermann, J. P.; Desfrancois, C. *J. Electron. Spectrosc.*
10
11 *Relat. Phenom.* **2000**, 106, 141.
12
13
14 (7) Lyapustina, S. A.; Xu, S.; Nilles, J. M.; Bowen, K. H. *J. Chem. Phys.* **2000**, 112, 6643.
15
16
17 (8) Wang, X.-B.; Nicholes, J. B.; Wang, L.-S. *J. Chem. Phys.* **2000**, 113, 10837.
18
19
20 (9) Morgado, C. A.; Pichugin, K. Y.; Adamowicz, L. *Phys. Chem. Chem. Phys.* **2004**, 6, 2758.
21
22
23 (10) Muraoka, A.; Inokuchi, Y.; Nishi, N.; Nagata, T. *J. Chem. Phys.* **2005**, 122, 094303.
24
25
26 (11) Tsukuda, T.; Saeki, M.; Kimura, R.; Nagata, T. *J. Chem. Phys.* **1999**, 110, 7846.
27
28
29 (12) DeLuca, M. J.; Niu, B.; Johnson, M. A. *J. Chem. Phys.* **1988**, 88, 5857.
30
31
32 (13) Tsukuda, T.; Johnson, M. A.; Nagata, T. *Chem. Phys. Lett.* **1997**, 268, 429.
33
34
35 (14) Shin, J.-W.; Hammer, N. I.; Johnson, M. A.; Schneider, H.; Glola, A.; Weber, J. M. *J. Phys.*
36
37 *Chem. A* **2005**, 109, 3146.
38
39
40 (15) Inokuchi, Y.; Nishi, N.; *J. Chem. Phys.* **2001**, 114, 7059.
41
42
43 (16) Gaussian 98, Revision A.11.4, M. J. Frisch, G. W. Trucks, H. B. Schlegel, G. E. Scuseria, M. A.
44
45 Robb, J. R. Cheeseman, V. G. Zakrzewski, J. A. Montgomery, Jr., R. E. Stratmann, J. C. Burant, S.
46
47 Dapprich, J. M. Millam, A. D. Daniels, K. N. Kudin, M. C. Strain, O. Farkas, J. Tomasi, V. Barone, M.
48
49 Cossi, R. Cammi, B. Mennucci, C. Pomelli, C. Adamo, S. Clifford, J. Ochterski, G. A. Petersson, P. Y.
50
51 Ayala, Q. Cui, K. Morokuma, N. Rega, P. Salvador, J. J. Dannenberg, D. K. Malick, A. D. Rabuck, K.
52
53 Raghavachari, J. B. Foresman, J. Cioslowski, J. V. Ortiz, A. G. Baboul, B. B. Stefanov, G. Liu, A.
54
55 Liashenko, P. Piskorz, I. Komaromi, R. Gomperts, R. L. Martin, D. J. Fox, T. Keith, M. A. Al-Laham, C.
56
57 Y. Peng, A. Nanayakkara, M. Challacombe, P. M. W. Gill, B. Johnson, W. Chen, M. W. Wong, J. L.
58
59
60

1
2
3 Andres, C. Gonzalez, M. Head-Gordon, E. S. Replogle, and J. A. Pople (Gaussian, Inc., Pittsburgh PA,
4
5 2002).

6
7
8 (17) Serrallach, A.; Meyer, R.; Günthard, Hs. H. *J. Mol. Spectrosc.* **1974**, 52, 94.

9
10
11 (18) Saeki, M.; Tsukuda, T.; Iwata, S.; Nagata, T. *J. Chem. Phys.* **1999**, 111, 6333.

12
13
14 (19) Cooper, C. D.; Compton, R. N. *J. Chem. Phys.* **1977**, 67, 1779.

15
16
17 (20) Saeki, M.; Tsukuda, T.; Nagata, T. *Chem. Phys. Lett.* **2001**, 340, 376.
18
19
20
21
22
23
24
25
26
27
28
29
30
31
32
33
34
35
36
37
38
39
40
41
42
43
44
45
46
47
48
49
50
51
52
53
54
55
56
57
58
59
60

Figure captions

Figure 1. Overview of the infrared photodissociation spectra of $[(\text{CO}_2)_n(\text{CH}_3\text{OH})_m]^-$ measured in the 2700 – 3700 cm^{-1} range. The numbers n - m in the figure denote the composition of $[(\text{CO}_2)_n(\text{CH}_3\text{OH})_m]^-$.

Figure 2. Optimized geometries for $[(\text{CO}_2)_1(\text{CH}_3\text{OH})_1]^-$ obtained at the MP2/6-311++G** level. Bond lengths and angles are given in units of Å and degree unless otherwise noted.

Figure 3. Optimized geometries for $[(\text{CO}_2)_2(\text{CH}_3\text{OH})_1]^-$ obtained at the MP2/6-311++G** level.

Figure 4. Infrared photodissociation spectrum of $[(\text{CO}_2)_3(\text{CH}_3\text{OH})_1]^-$ (top panel) compared with the calculated vibrational spectra for $[(\text{CO}_2)_3(\text{CH}_3\text{OH})_1]^-$ isomers. One unit in the ordinate of the calculated spectra corresponds to the IR intensity of 1500 $\text{km}\cdot\text{mol}^{-1}$. Also shown on the right side are the corresponding optimized structures of the $[(\text{CO}_2)_3(\text{CH}_3\text{OH})_1]^-$ isomers.

Figure 5. Infrared photodissociation spectrum of $[(\text{CO}_2)_1(\text{CH}_3\text{OH})_2]^-$ (top panel) compared with the calculated vibrational spectra for $[(\text{CO}_2)_1(\text{CH}_3\text{OH})_2]^-$ isomers. One unit in the ordinate of the calculated spectra corresponds to the IR intensity of 1500 $\text{km}\cdot\text{mol}^{-1}$. Also shown on the right side are the corresponding optimized structures of the $[(\text{CO}_2)_1(\text{CH}_3\text{OH})_2]^-$ isomers.

Figure 6. Infrared photodissociation spectrum of $[(\text{CO}_2)_2(\text{CH}_3\text{OH})_2]^-$ (top panel) compared with the calculated vibrational spectra for $[(\text{CO}_2)_2(\text{CH}_3\text{OH})_2]^-$ isomers. One unit in the ordinate of the calculated spectra corresponds to the IR intensity of 1500 $\text{km}\cdot\text{mol}^{-1}$. Also shown on the right side are the corresponding optimized structures of the $[(\text{CO}_2)_2(\text{CH}_3\text{OH})_2]^-$ isomers.

Figure 7. Infrared photodissociation spectra of $[(\text{CO}_2)_n(\text{CH}_3\text{OH})_1]^-$ ($n = 4 - 7$). The solid lines represent the experimental data. The dotted curves are the Lorentzian components in the spectral deconvolution processing. The digits “0”, “1” and “2” indicate the components attributed to the isomeric forms of categories I^0 , I^1 and I^2 , respectively.

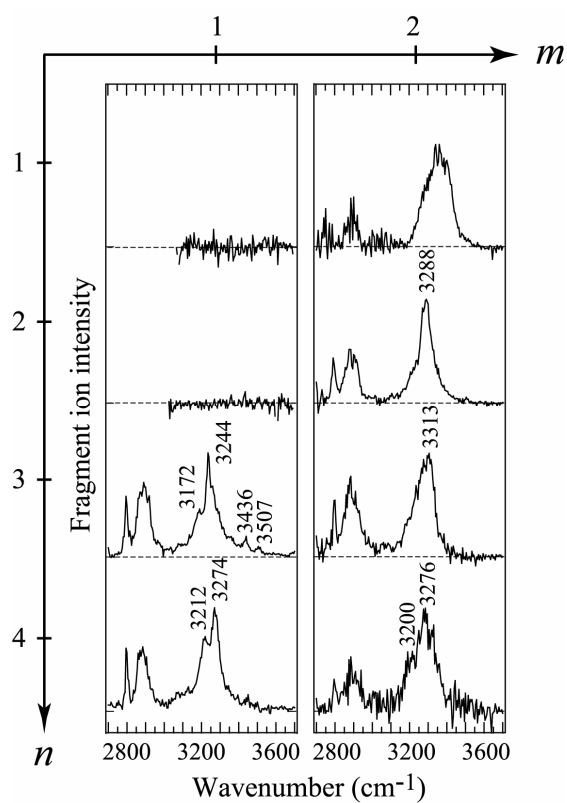


Figure 1. Muraoka *et al.*

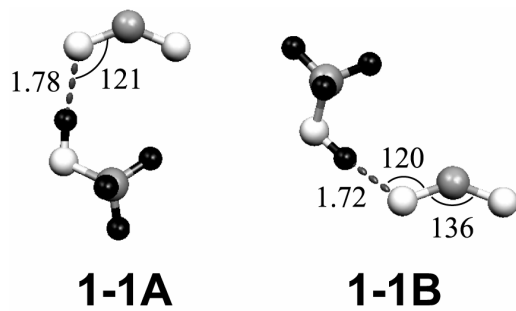


Figure 2. Muraoka *et al.*

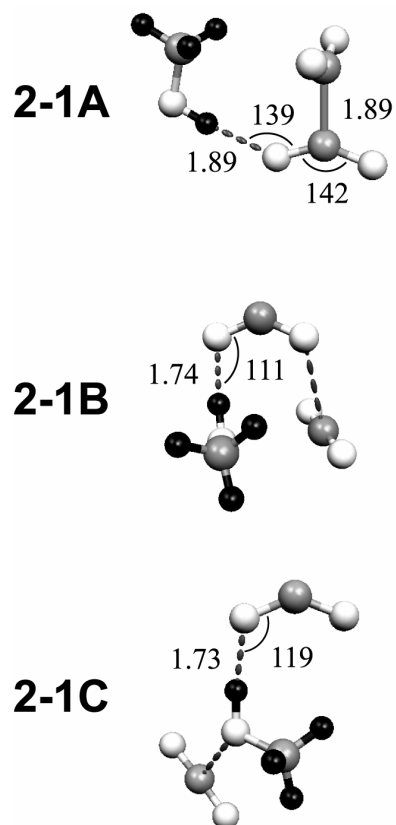


Figure 3. Muraoka *et al.*

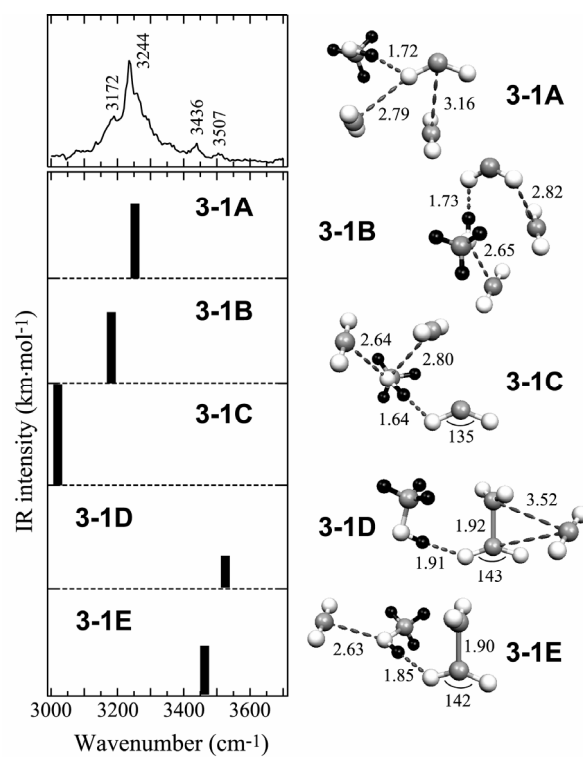


Figure 4. Muraoka *et al.*

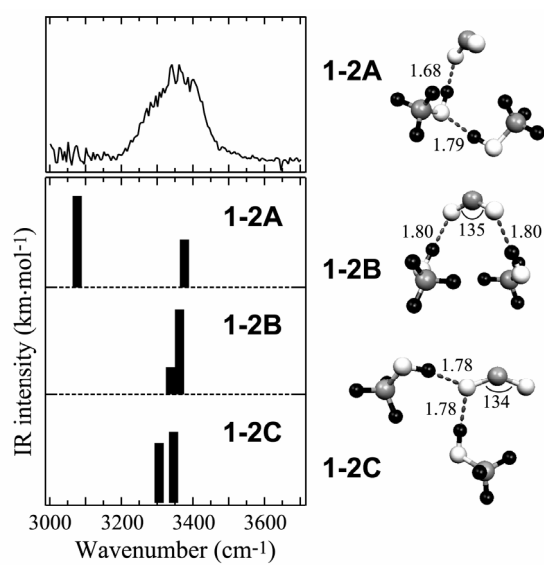


Figure 5. Muraoka *et al.*

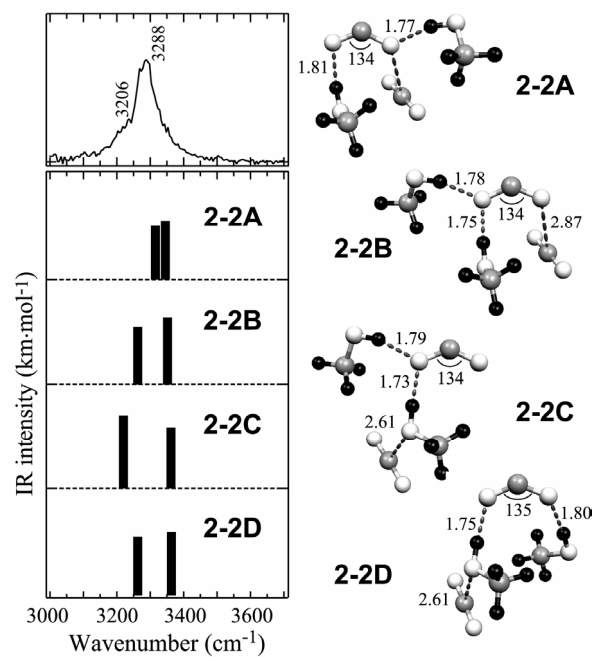


Figure 6. Muraoka *et al.*

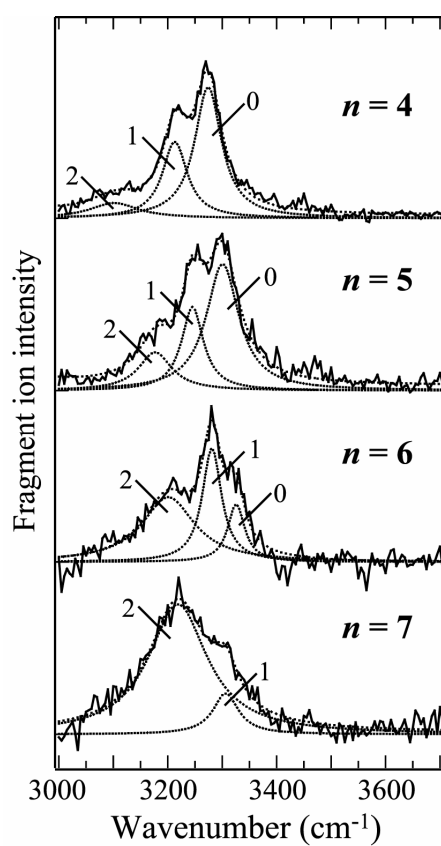


Figure 7. Muraoka *et al.*